Muñoz-García, M.-Á., Fouris, T., & Pilat, E. (2021). Analysis of the soiling effect under different conditions on different photovoltaic glasses and cells using an indoor soiling chamber. *Renewable Energy*, *163*, 1560–1568. doi: 10.1016/j.renene.2020.10.027

Journal Pre-proof

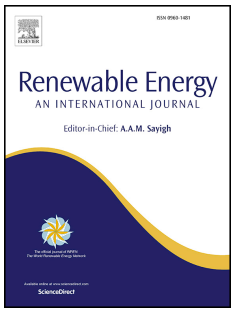

Analysis of the soiling effect under different conditions on different photovoltaic glasses and cells using an indoor soiling chamber

Miguel-Ángel Muñoz-García, Tom Fouris, Eric Pilat

PII: S0960-1481(20)31593-7

DOI: https://doi.org/10.1016/j.renene.2020.10.027

Reference: RENE 14317

To appear in: *Renewable Energy*

Received Date: 11 July 2020

Revised Date: 1 October 2020

Accepted Date: 6 October 2020

Please cite this article as: Muñoz-García Miguel-Á, Fouris T, Pilat E, Analysis of the soiling effect under different conditions on different photovoltaic glasses and cells using an indoor soiling chamber, *Renewable Energy* (2020), doi: https://doi.org/10.1016/j.renene.2020.10.027.

Analysis of the soiling effect under different conditions on different photovoltaic glasses and cells using an indoor soiling chamber

Miguel-Ángel Muñoz-García[1*†], Tom Fouris[2,3], Eric Pilat[2]

[1] Universidad Politécnica de Madrid, Madrid, Spain
[2] CEA-INES, LSPV (Systems Laboratory) France
[3] INSA (National Institute of Applied Sciences), Rennes, France

The effects of deposition of dust (soiling) on photovoltaic (PV) modules, mainly on their energy production, is a topic that is gaining importance, related to the increase in PV installations in very sunny arid areas and, therefore, which theoretically lead to higher energy production. Due to the multitude of influent factors regarding soiling experiments, the use of a climatic chamber dedicated to the study of soiling is a subject of great interest.

This work presents a methodology to reproduce the soiling process and the analysis of its effects, using optical and electrical approaches. The experiments included simulating different climatic conditions representative of the desert climate. In total, 19 replicates were performed for three different experiment conditions on five different glasses and two solar cells. Different glass samples, with different anti-soiling treatments, have been used to measure optical transmittance losses and to examine deposition by microscopy, while photovoltaic cells have been used to quantify electrical losses.

The dust load ranged from 1.30 to 1.63 g/m^2 promoting electrical losses from 4.73 to 6.90% depending not only on the dust load but also on the conditions in which it was deposited.

KEY WORDS: Soiling, Soiling chamber, Anti-reflective glass, Anti-soiling glass

1. Introduction

1.1.Soiling causes loss of electricity production

The effect of soiling in a photovoltaic system is mainly the loss of solar radiation that reaches the cell and, therefore, a decrease in the production of electricity. This is the main impact, but not the only one. Different studies determined that, depending on the area where the solar plant is located, it can imply a loss of 1% per day, and accumulated during dry periods can reach 40% [1] or up to 60% [2] causing significant losses [3], [4].

Other undesirable effects caused by soiling include the possibility of the appearance of hot spots, due to the shading effect of the dust on some parts of the module, which could cause long-term degradation promoted by the dust cementation.

Different works have analysed the causes and effects of soiling. The combination of factors plays an important role in the deposition of the dust in the panels. The angle of incidence [5], must be taken into account in fixed module plants, where according to experiments, the losses vary from 2.3% under normal incidence (0º) of the light to the panel, to 8% when the angle is

* Correspondence to: Miguel-Ángel Muñoz-García, Universidad Politécnica de Madrid.
Dep. Ing. Agroforestal-Electrotecnia y Energías Renovables. LPF-TAGRALIA.
Avda. Complutense s/n, 28040 Madrid, Spain
† E-mail: miguelangel.munoz@upm.es

58º. Also the formation of dew during the night or at dawn, is a factor that drastically influences the deposition of dust and causes cementation.

1.2. Influence of natural factors and system design

Soiling on a PV module is a complex issue because of the number of factors that influence deposition, in addition to the bonding forces of particles to the front sheet of PV panels [6]. Ilse et al. [7] noticed the high heterogeneity regarding the different scales of these factors that can be linked to the dust, the module and the environment. Many studies seem to assign the particle size parameter as one of the most influential factors and PM2.5 and PM10 (airborne particles with a diameter less than or equal to 2.5 μm and 10 μm, respectively) are the primarily responsible for covering the surface of the modules [6]–[11]. Due to their lightness, these 2.5 μm particles can travel long distances [12] and there are some well-known dust sources such as the deserts of the Middle East [13], the Sahara desert [14]–[16] or the Asiatic deserts [14] from where the particles could be emitted. The diameter of the particles is a parameter that we must consider to perform some analysis regarding soling.[15]

All these particles, but also the dust that can be found around the site of the PV plant, can accumulate on the PV modules. The adhesion of the particles is due to various forces such as Van der Waals, capillary, electrostatic and gravitational forces [16], [17].

The sources of dust but also the location of the modules, are important because they will determine the composition of the dust and, consequently the phenomena of bonding, cementation, caking, and capillary. Several studies present an interaction between the soiling rate and the dust composition [7], [18], [19]. The cementation process occurs after deposition and requires more time to make the particles to fix well on the module. In general, cementation seems to be highly related to relative humidity (RH) in the environment where the modules are located [16]–[18]. Depending of humidity and temperature, dew may appear [20] on the modules and a thin film of water will increase the adhesion forces responsible for the cementation of the particles [21]–[23]. This factor also needs attention in indoor soiling studies. Understanding these parameters could lead to some prediction models for soiling losses.[24].

At the module scale, its characteristics also have an impact on the adhesion of particles, especially with respect to the glass surface. For some years now, some glass manufacturers are trying to develop different special anti-soiling coating to mitigate the problem [25]–[27].

2. Objectives of the work

The objective of this work is to simulate different soiling situations, in different solar cell glasses treated with different coatings, suggesting a methodology to carry out tests in an indoor chamber. In addition to this, not only glasses but also two whole cells of the same heterojunction technology (HET) but with a different glass treatment were analysed in order to assess the differences.

The objectives can be summarized as:

- What is the effect of dry soiling at different temperatures?
- How does dew influence the impact of soiling?
- What is the relationship between soiling and the electrical response of a cell?
- How does direct optical transmission correlate with Isc drop?

3. Materials and Methods.

3.1.The soiling chamber

The main tool is a dedicated chamber developed by CEA. It consists of a 100 cm x 60 cm x 50 cm rectangular base enclosure of with temperature and humidity control. Inside the chamber, air temperature and relative humidity are controlled by a PID controller. It includes two fans on both sides of the chamber (see Figure *1*). Within this enclosure, air and sample temperatures, and relative air humidity are monitored using a GL240 and a EL-GFX-2 data-loggers.

Figure 1.- Chamber internal view (left),and external view (right)

The temperature of the samples was controlled by a different system based on water flowing inside the sample holder, whose temperature was controlled through an external cooling/heating system. Therefore, samples and air temperatures were independently controlled.

The dust (soil) used for the experiments was the standardized ARIZONA ISO 12103-1 composed mainly of silica and various metal oxides (see Table *1*), which are often found in quartz and feldspar minerals. This soil is forced inside the chamber by using an RBG 1000 dust diffuser (see Figure 2). The diffuser spreads the dust in the chamber using a rotating brush and an air pressurized volumetric dust feeding device. Upon reaching the chamber, the soil is projected onto a deflector to generate a homogeneous cloud above the tested sample. The samples are placed on a tilting heating or cooling plate, according to the scheme presented in Figure 3.

Figure 2: RBG 1000 dust generator

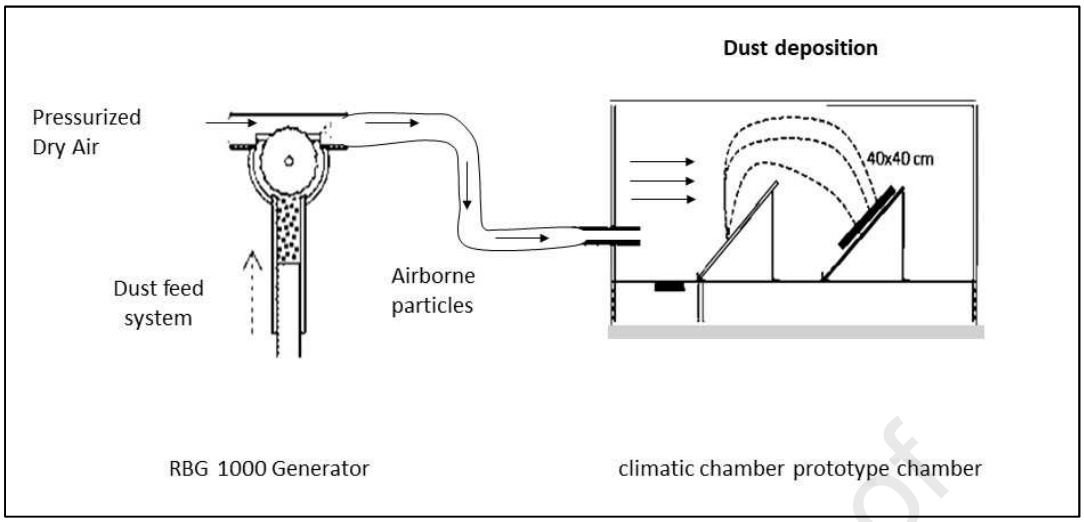

Figure 3: schema of the process used for indoor artificial soiling

CAS No	Components	Quantity
14808-60-7	Silica (fine dust)	69-77%
1344-28-1	Aluminium oxide	8-14%
1305-78-8	Calcium oxide (mineral)	2.5-5.5%
12136-45-7	Potassium oxide (mineral)	2-5%
1313-59-3	Sodium oxide (mineral)	1-4%
1309-37-1	Iron (III) oxide (hematite)	4-7%
1309-48-4	Magnesium oxide	1-2%
13463-67-7	Titanium dioxide	0-1%

Table 1.- Arizona Dust Components list (according to 29 CFR 1910.1200 (g))

3.2.Experiments setup and test samples used

In order to simulate representative extreme situations in desert regions, three different climate configurations are reproduced within the chamber as shown in Table 2.

Name	Experiment type	Air temperature (°C)	Sample temperature (°C)	Relative Humidity (%)
Experiment1: 30_60_20	ARID	30	60	20
Experiment2: 10_5_80	DEW	10	5	80
Experiment3: 25_25_40	MID	25	25	40

Table 2.- Different experiments carried out.

These experiments reproduce some of the different situations that would occur in desert regions. Experiment 1 would be similar to the beginning of a sunny day, with a big difference between the solar module and the air temperatures. In addition to this, Experiment 2 reproduces the dew point phenomenon, which would occur mainly at the end of the night, when there is thermal inversion between the temperatures of the solar modules and the air. During the night, the cells are dissipating their heat (IR radiation) towards the sky and, as a consequence, after a few hours, the panel temperature would be lower than the air temperature. Finally, Experiment 3 represents a case in which the balance between the air and the solar module temperatures occur, which would occur on a cloudy but relative dry day.

The test samples were chosen as follows:

Glass family: 50 x 50 mm, 2 mm thickness: There are 5 different glasses, each with its own glass quality and coating treatment. Sample glasses include: plain glass (non-photovoltaic), untreated photovoltaic glass, anti-reflective treatment glass, hydrophobic glass and anti-reflective/anti-soiling glass.

Single-cell module family: 160 x 160 mm glass-glass Glass-glass, 5 mm thickness (see Figure 4). There are two different modules, both include the same cell technology, but each with its own glass quality and coating treatment: no treatment and an anti-soiling treatment.

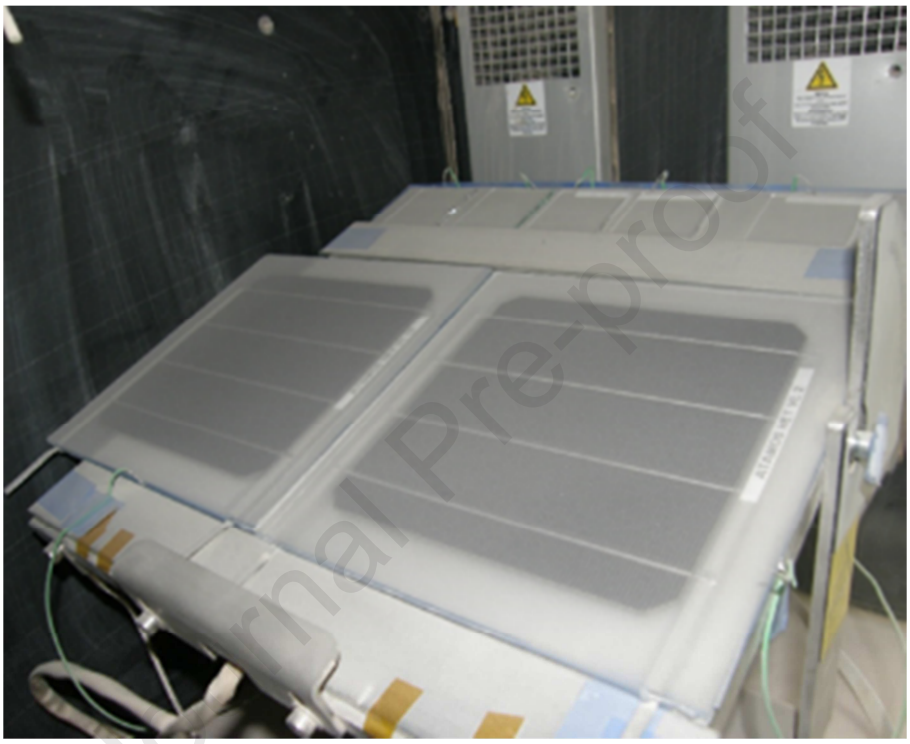

Figure 4: Five glass samples (upper part) and two cell modules (lower part) on the tilted plate inside the chamber after soiling

The deposited dust was weighed using a precision balance to observe and compare the amount of deposited dust per sample, and then calculated per cm^2 or per m^2 for the different experiments. To do this, the samples were weighed before and after each experiment.

3.3.Transmittance tests

There is a direct relationship between the optical transparency of the cell glass and the current generated by the cell itself. To obtain the optical transmission response, the five glass samples used for the tests were analysed by spectrophotometry. The spectrophotometer used was Shimadzu UV 2600, which wavelength range in direct transmission is 300-900 nm with a resolution of 0,1 nm:

The relation between optical transmission and photovoltaic efficiency is not obvious. First, the transmitted light is formed by direct and scattered light, but the use of a spectrometer only considers direct light transmission, and second, the spectral response of cell technology favours some wavelengths over others.

Before artificial soiling begins, in the glass family, all samples are cleaned, and direct transmission is measured.
Figure 5 shows the spectrophotometric results for each type of glass.

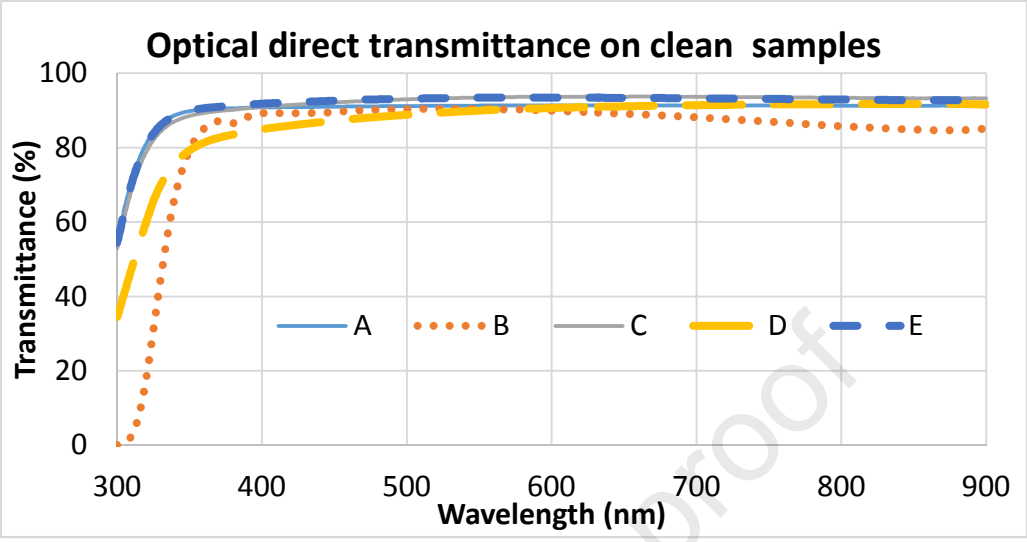

Figure 5: Optical direct transmittance curves obtained through cleaned glass samples

We can see that glass B does not allow transmission of wavelengths below 350 nm. This type of low-cost standard glass does not benefit from the specific manufacturing process with low contamination by iron particles. In addition, we see that glass D is significantly less transparent than others, especially below 500 nm.

3.4.Electrical parameters analysed

The electrical impact is assessed by measuring the Isc drop due to the effect of soiling. Tests carried out on CEA flash solar simulator are at STC conditions (Tcell=25 ºC, G=1000 W/m^2, spectrum: 1.5 AM), Isc (short circuit current) is directly affected by soiling, as it is directly proportional to the incident radiation. The flash solar simulator is a Pasan class AAA tester with an accuracy of ± 0,5%.

Indeed, the current generated follows the following equation [28] :

$$I = I_L - I_o\left(e^{\frac{[V+IRs]}{mVt}} - 1\right) - \frac{[V+IRs]}{Rp} \quad \text{Equation 1}$$

Where I_L is the photocurrent generated at the cell junction, and I is the current obtained outside the cell, which is affected by the series and the parallel resistances (Rs and Rp), the working voltage V and the current of the diode Io, as well as temperature.
In normal operation, I goes from 0 (open circuit) to Isc (short circuit current). Focusing in Isc, it varies with radiation (G) and temperature (T) and any comparison should be made at STC, so Isc should be translated into I^*_{sc} (short circuit current at STC) using the following formula [29], [30]:

$$I^*_{SC} = I_{SC}\left(\frac{G^*}{G}\right) - \propto (T - T^*) \quad \text{Equation 2}$$

In $I_{SC}^{*} = I_{SC}\left(\frac{G^{*}}{G}\right) - \propto (T - T^{*})$ Equation 2, G*,T* and I^{*}_{SC} are the radiation, temperature and short-circuit current at STC, while G, T and I_{SC} are the actual measured radiation, temperature and short-circuit current, respectively. Also, the α constant is intrinsic to the cell. In fact, the cell current variation is proportional to its Isc variation, according to EN-60891 and the formula [29], [31]:

$I_2 = I_1 + I_{SC}\left(\frac{G_2}{G_1} - 1\right) + \propto (T_2 - T_1)$ Equation 3

In Equation 3 I_1 is the current measured at a given G_1 radiation and T_1 temperature used to calculate what would be the current that would be measured at a given G_2 radiation and T_2 temperature. To decrease the measurement uncertainty, for each experiment, at least 2 measurements are performed for the Isc and the analysis results are the mean value. To confirm the good temporal stability of the measurement, the samples are cleaned and tested again at the end of the experiment, to confirm that the result obtained is close enough to the previous one, before the soiling operation.

3.5.Image processing and particle counting.

In addition to spectrophotometric analysis, we developed and evaluated an image processing measurement methodology with the aim of determining the soiling coverage ratio. The tools used were a Keyence digital microscope and ImageJ software.

The microscope captured the images, at magnification up to x1000. To minimize the spatial distribution error, 5 points including the sample centre and the corners were analysed for each sample under test. Then, the mean and variance of the samples were evaluated to ensure the validity of the test.

The magnification of the image depends on how the dust is distributed on the glass surface. For example, in Experiment 2, dew generated clean channels on the glass (see Figure *6*) and high-magnification images (x1000) taken inside or outside of these channels may be inconsistent. In this case, a lower magnification (x200) is considered more relevant.

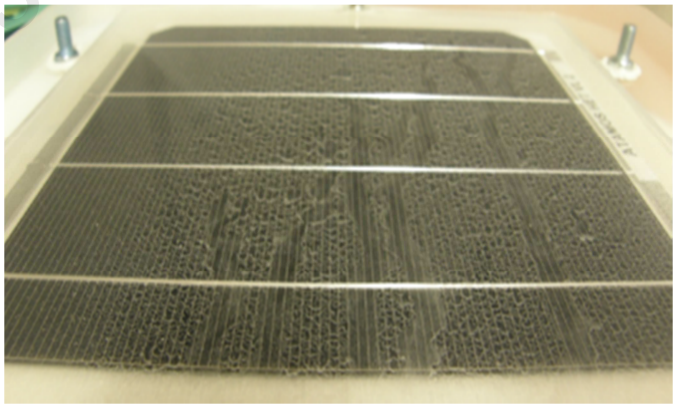

Figure 6.- Water channels on the glass surface because of dew

The images in Figure 7 show the three stages in processing the x1000 image, from the original image to the filtered image, and finally after the threshold. In this case, the coverage percentage was 13.9%. The case shown is one of the dry tests with high temperature differences between the sample and the air.

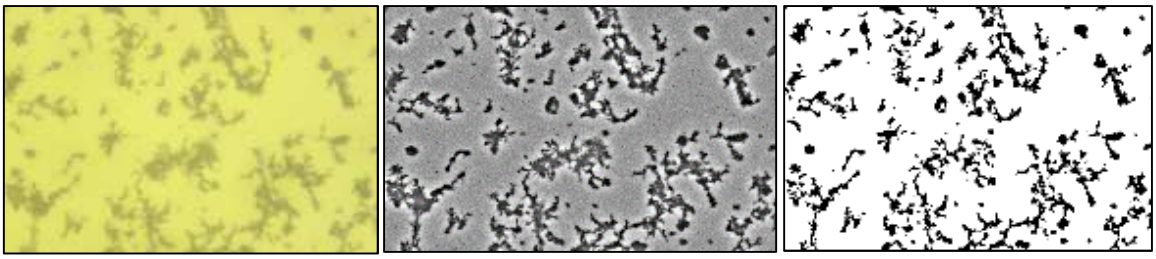

Figure 7.- Original (left), filtered image (middle) and processed (right) x1000 images of glass type E

In the case of wet tests, where the dew point was reached, the pre-filtering was not convenient as it was for the tests mentioned above, and the amplification x200. Then a "Threshold" and a "Particle Count" commands were applied. The images in Figure 8, show the stages in the x200 image processing. The coverage calculated using this method was 28.5%.

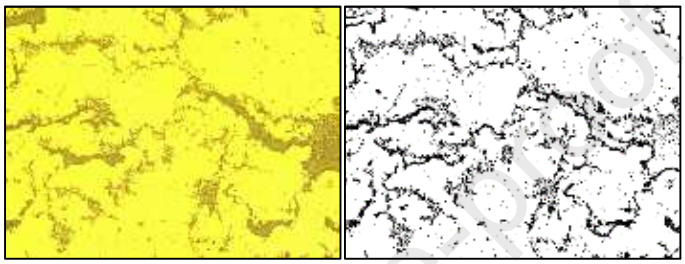

Figure 8.- Original and processed x200 images of glass type C

4. Results and discussion

Three different environmental conditions were simulated, to analyse the different desert conditions during the day and at night, named "30_60_20", "10_5_80", and "25_25_40" as mentioned above. Only at "10_5_80" did the temperature difference combined with the relative humidity promote condensation on the surface of the samples. In total, 19 repetitions including different experiments were performed inside the chamber. Each of them included weighing, spectrophotometry, image analysis and I-V curve analysis.

The samples were weighed before and after each experiment in order to obtain the weight of the deposited dust, and the mean values for all the samples were obtained for each experiment (see Figure *9*). Even though the accumulated dust is not very high, it is comparable to low soiling rate situations that appear after a few days of exposure. Furthermore, the load is consistent with the loss of transmittance. The analysis of this point will be made later.

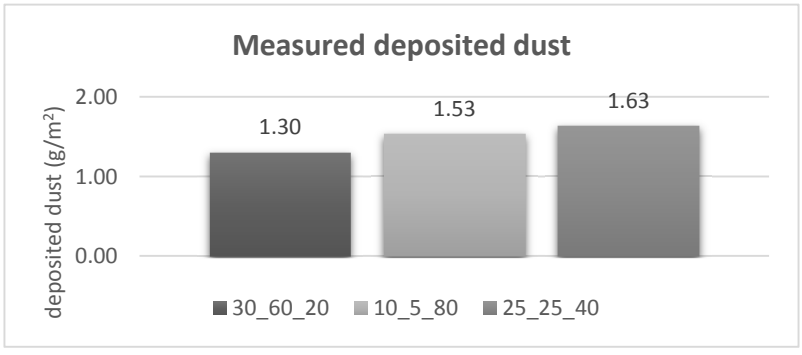

Figure 9 Dust deposited after each experiment.

4.1.Analysis of direct transmittance after dust deposition

Direct transmittance measurements showed a significant drop in the three cases studied, for all samples analysed. We can observe this drop for each type of glass and for each experiment. According to the results, the highest drop occurred in the experiment “25_25_40” (T-air= 25 ºC, T-cell=25 ºC and RH= 40%) and the lowest in the experiment “30_60_20” (T-air= 30 ºC, T-cell=60 ºC and RH=20%) and that is confirmed regardless the type of glass.

Figure *10* shows the transmittance curves resulting from the experiment “30_60_20” and *Figure 11*, those resulting from the experiment “25_25_40”. The main difference between the setting of these two experiments is the temperature of the glass. The results clearly show that this temperature parameter significantly mitigates the optical impact of soiling deposition.

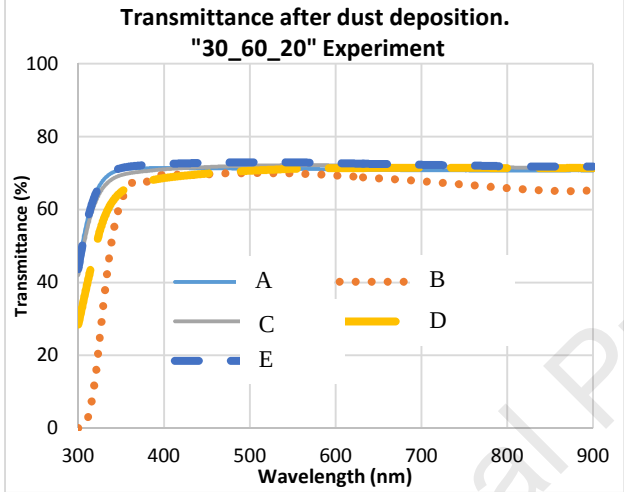

Figure 10.- Direct optical transmittance after dust deposition in dry and hot conditions

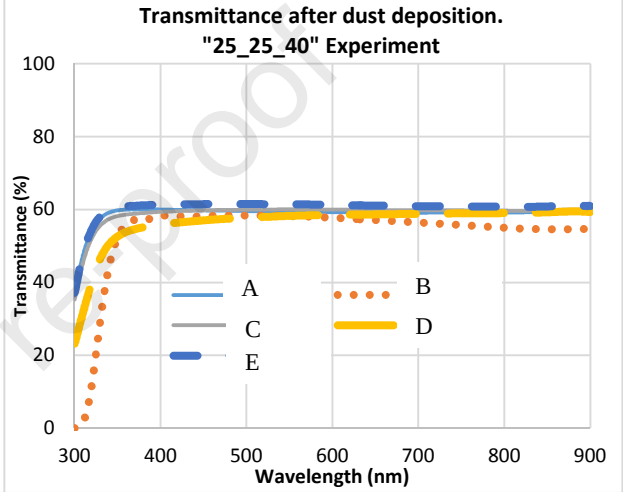

Figure 11.- Direct optical transmittance after dust deposition in dry conditions when T-cell and T-air are similar

Regarding the experiment “10_5_80”, where the dew point was reached, the results were not as homogeneous as for other experiments, showing important differences depending on the type of the glass. Then, in Figure 12 it can be seen that glass E is more efficient, showing less loss of direct transmittance compared to those of C and D.

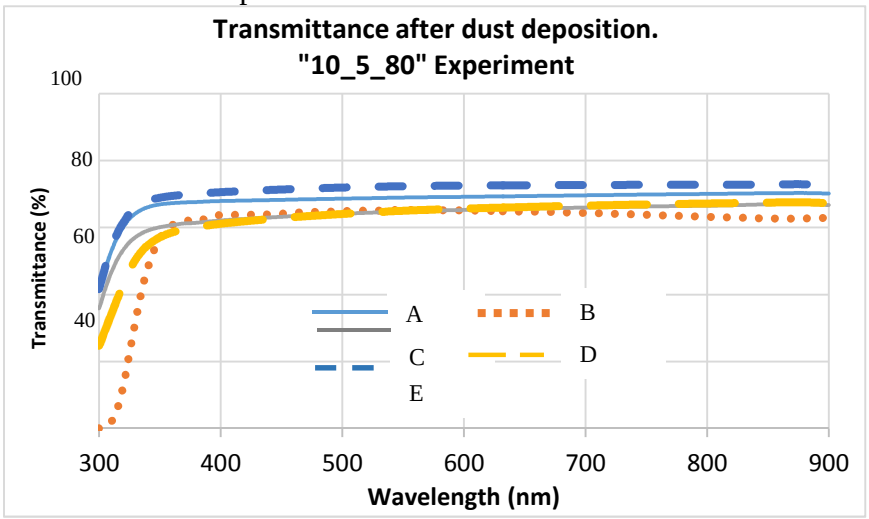

Figure 12.- Direct optical transmittance after dust deposition when dew point is reached

The figures above show the effect of soiling on the direct optical transmittance curves for each experiment. As already mentioned, the direct transmittance presented up to now, is not weighted according to the spectral response of any cell. However, if we compare the results in Figure *9* with the results in Figure *10*, Figure *11*, and Figure 12, the dust load and direct transmittance are related, as expected. In the next section, direct transmittance is related (weighed) to the spectral response of cells, which is used in the family of samples from single-cell modules.

4.2.Comparing soiling optical effects using the spectral response

The direct transmittance drop was high (20-30%) for both dry cases, compared to the original data under clean conditions. This effect must consider the spectral response of the solar cell where each of the glasses would be used. Therefore, a further analysis was performed to consider the spectral response of a HET cell. Relative transmittance loss, multiplied by the Spectral Response (SR), also known as responsivity, and standard irradiance (AM1.5) at a given wavelength G(λ) were used.

Depending on the responsivity of the cell, the transmittance at some wavelengths will impact more or less than at other wavelengths. The responsivity is generally determined in units such as photo-current density generated to the incident radiation at a given wavelength, following the formula [32]:

$$SR(\lambda) = \frac{J_{ph}(\lambda)}{G(\lambda)} \ [\frac{A}{W}] \qquad \text{Equation 4}$$

In this equation, Jph is the density of the photocurrent in A/m^2, and G is the incident radiation in W/ m^2, both at a each wavelength λ. To be used, it is generally related to the quantum efficiency (QE), defined as the number of charge carriers collected by a cell due to the flux of the incident photon [33], and follows the next formula:

$$QE\ (\lambda) = \frac{J_{ph}(\lambda)/q}{n_{ph}} \qquad \text{Equation 5}$$

Where QE is the quantum efficiency or the electrons obtained per photon, q is the charge of the electron in Coulombs and n_{ph} is the photons flux in photons/s-m^2. Then, using the Plank-Einstein equation (E=hν=hc/λ) and the values for the Plank's constant (h), the speed of light (c), and the wavelength λ of the incident photon, the formula can be simplified as:

$$SR\ (\lambda) = \frac{QE(\lambda) * \lambda(\mu m)}{1.23985\ (\mu m\ W/A)}\ [A/W] \qquad \text{Equation 6}$$

Finally, for our purposes, we will apply the SR on a given λ multiplied by the loss of transmittance Td(λ) and by G(λ) to obtain a relative value of the influence of the decrease in transmittance for each experiment, on the loss of current density obtained, summarized in the formula:

$$Jd\ (\lambda) = Td(\lambda) * SR(\lambda) * G(\lambda) \qquad \text{Equation 7}$$

The calculation uses the normalized transmittance loss (relative to clean glass conditions), so Td(λ) is the relative decrease and, as a result, the above formula provides the decrease in the density of the photo-current.

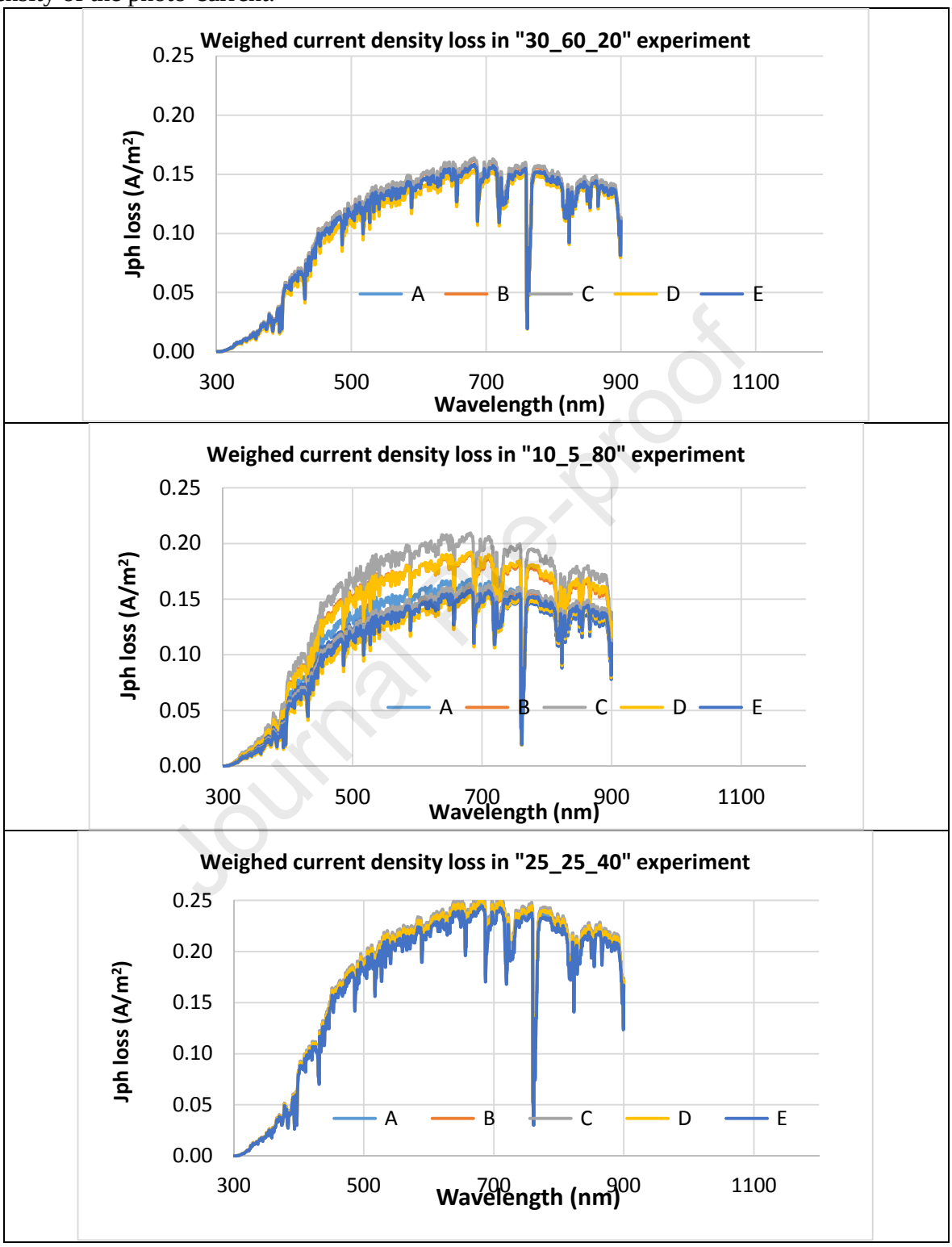

Figure 13. Calculated current density loss by applying direct transmission to spectral response.

Figure 13 shows the calculated current density loss for each wavelength for the different experiments and glasses. The calculation considers not only direct transmission loss but also spectral response and the AM1.5 radiation. As indicated above, direct transmission is related to the generated photocurrent, but indirect transmission must also be considered for the actual

current generated. However, all the samples are tested under the same conditions, so the comparison is valid to see differences between them. According to the results, the main conclusion is the confirmation of the higher losses in the experiment "25_25_40".

By integrating the curves shown in Figure 13, the theoretical weighed short-circuit current loss, related to the direct transmittance drop, is obtained, with the only limitation of the wavelengths considered due to the limits of the spectrophotometer used in the experiments. However, when calculating the weighed short-circuit current in clean conditions, also for the same wavelength constraints, a comparison of the current generated in clean and dirty conditions is of a great interest.

$$I_{sc-loss}\,(\lambda_1 - \lambda_2) = \int_{\lambda_1}^{\lambda_2} Td(\lambda) * SR(\lambda) * G(\lambda)\, d\lambda \qquad \text{Equation 8}$$

Using this equation and normalising with the Isc calculated under clean conditions, the results obtained for different experiments are presented in the following table:

	Calculated theoretical relative (300-900 nm) Isc drop				
Experiment	A	B	C	D	E
30_60_20	23,53%	24,07%	24,32%	22,36%	23,48%
10_5_80	24,22%	24,22%	24,22%	24,22%	24,22%
25_25_40	34,88%	35,61%	35,78%	35,28%	34,27%

Table 3.- Isc normalised theoretical drop of for all the glasses analysed, from 300 to 900 nm.

The previous results have only considered the direct transmission weighed by the spectral response, so these curves only take into account the optical losses measured through the glass. In the next section, the results of the effective influence of soiling on the produced current will be presented, when the actual short-circuit current is measured.

4.3.Indoor flash solar simulator for Isc measurement

Looking at the three experiments, the measured short-circuit current suffered a significant drop in all of them. If we look at the differences in the results for the two cells of each experiment independently (Figure 14), we can conclude that the difference is not significant if we consider the measurement uncertainty. Experiment "10_5_80" (dew point reached) had the lowest current drop and experiment "25_25_40" (a similar temperature for cell and air), the highest.

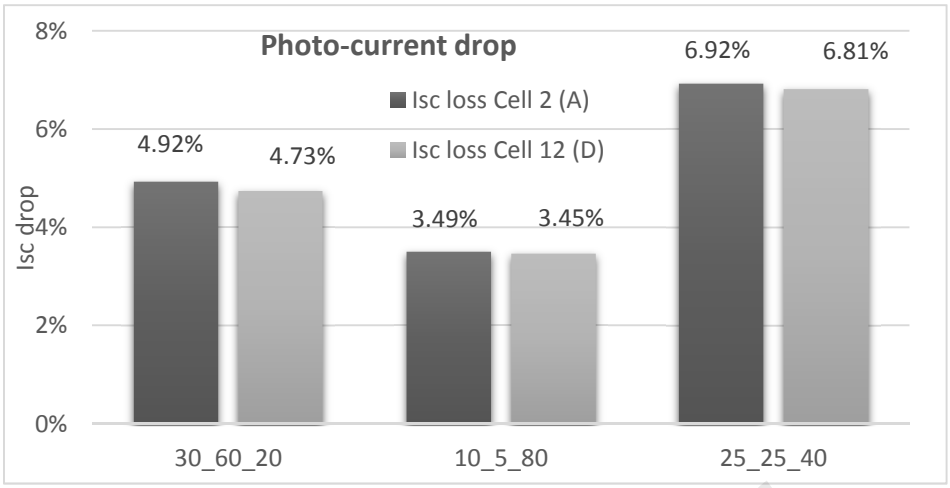

Figure 14.- Isc drop measured for the two samples in the different experiments for the two cells.

Compared to the weighed transmission losses, the actual Isc losses are not that high. This could be related to scattered light, which is not detected by transmittance analysis. Table 4 shows results and we can see that treatment D presents a better performance, mainly when cell temperature is high (30_60_20 experiment).

	Measured Isc drop		Δ(A-D)
	Cell2 (glass A)	Cell12 (glass D)	
30_60_20	4,92%	4,73%	0,19%
10_5_80	3,49%	3,45%	0,04%
25_25_40	6,92%	6,81%	0,11%

Table 4.- Isc drop for the analysed cells.

4.3.1. Current loss calculated by using direct transmittance and its relation to the measured Isc drop

One of the objectives of this work was to find a correlation between the loss of direct transmittance, weighted by the spectral response, and the actual current drop of the cells. As explained above, the theoretical results of this analysis are shown in Table 3.
For the actual Isc drop, we calculated the difference between the Isc measurements under clean conditions and after the experiments (Table 4).
In Figure 15 we compare both results and can see that the direct transmittance drop fits well with the short-circuit current drop, even if a significant difference is observed for the high humidity configuration experiments. This difference is probably due to the “water channels” already mentioned and described above.

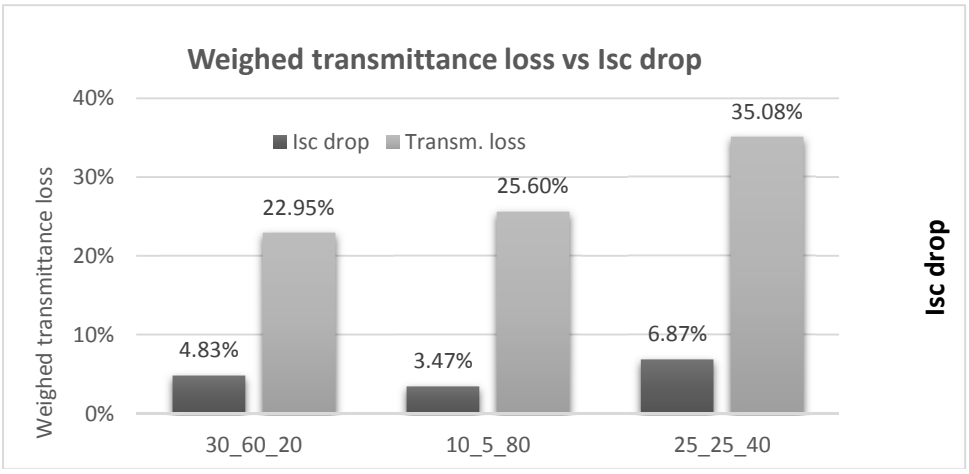

Figure 15.- Relationship between weighted direct transmittance drop and short-circuit current drop (Isc) for the three experiments

4.4.Image analysis, for the different experiments

When an image analysis of the surface covered by the dust was carried out for the three situations studied, as it happened in the case of losses of current and transmittance, the results were different for the dry and wet cases.

Figure 16 shows the percentage of the surface of the two analysed cells, using the aforementioned image analysis technique. The percent coverage for each sample was related to the transmittance analysis to determine the light blockage due to the dust cover. However, the coverage obtained using the mentioned strategy was only valid for dry experiments (30_60_20 and 25_25_40).

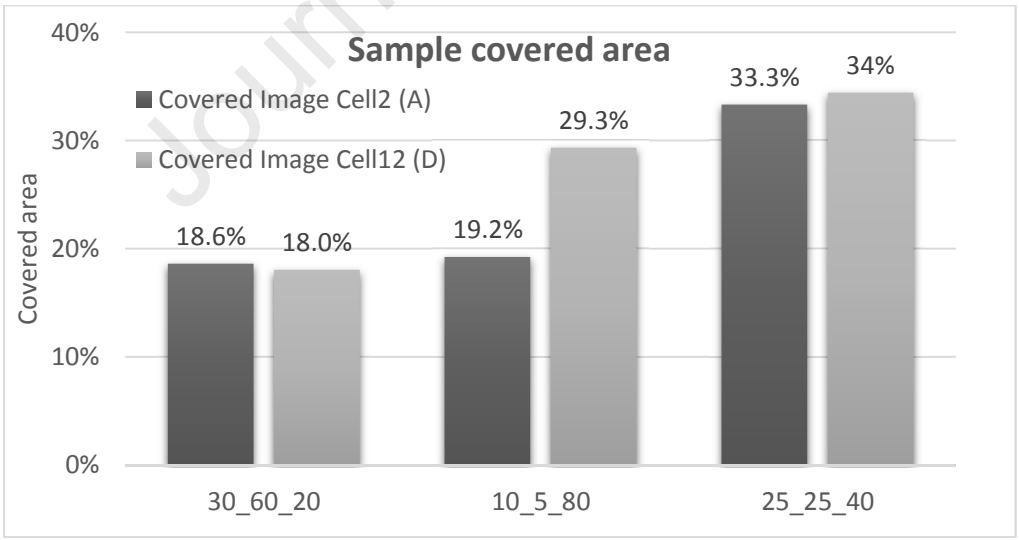

Figure 16.- Image analysis of the particle cover for the two samples in the three experiments.

The reason was probably the lack of homogeneity of the image after the wet test (10_5_80), which made the analysis by microscopy difficult. Then, according to the results, there was a correlation between the coverage obtained by the image analysis and the other variables: current and transmittance losses for experiments 30_60_20 and 25_25_40, but not for experiment 10_5_80. This finding can help in using the image analysis technique combined with an analysis of environmental conditions in order to determine if dew point was not reached and then to stablish the relationship between the covered surface and the current drop.

5. Conclusions

Experiments were carried out to analyse the effect of soiling, using an indoor chamber. The data obtained were studied, and different conclusions can be reached for the different analysed situations, including different temperature gradients between glass, cells and air, and different situations of relative humidity that reach or do not reach the dew point.
The indoor soiling chamber is considered a valuable tool to analyse the soiling effect simulating different test conditions. In this sense, the experience can serve to improve the chamber and intensify its use.
Taking into account the constraints of the conditions of the experiments, such as the size of the samples and the bandwidth of the spectrophotometer, interesting findings are obtained.

- Temperature of the module seems to mitigate the soiling optical impact. It was observed in all the glasses how the highest the temperature, the lower the soiling.
- When dew point is reached, a so called "water channels" appear on the glass and, as a consequence, the spectrophotometry or images measurement are not consistent enough to get a good correlation with the Isc drop. In this case, a deeper study could find relationships between reaching the dew point and non-uniformities in Isc drop.
- Cumulated soiling load of 1 to 2 g/m^2 can promote current losses in the cell from nearly 5% to 7%, but it is affected by the appearance of water channels in the surface, what can mitigate the loss.
- The correlation between short circuit current (Isc) drop and the optical direct transmittance measurement, weighed by the spectral response, has been demonstrated if the dew point is not reached. This can be used as a methodology to obtain one from the other.

6. Acknowledgments

The authors acknowledge the research support and the supply of equipment from the National Solar Energy Institute (CEA- INES), and to Universidad Politécnica de Madrid (UPM) for the support with the researcher's mobility program.

References

[1] Nimmo and Said, "Effects of dust on the performance of thermal and photovoltaic flat plate collectors in Saudi Arabia - Preliminary results - NASA/ADS," *Altern. Energy Sources*, vol. 1, 1979, Accessed: Dec. 02, 2019. [Online]. Available: https://ui.adsabs.harvard.edu/abs/1981aes.....1..145N/abstract.

[2] E. Asl-Soleimani and Farhangi, "The effect of tilt angle, air pollution on performance of photovoltaic systems in Tehran," *Renewable Energy*, vol. 24, pp. 459–468, Nov. 2001, doi: 10.1016/S0960-1481(01)00029-5.

[3] J. Zorrilla-Casanova *et al.*, "Analysis of Dust Losses in Photovoltaic Modules," *World Renewable Energy Congress 2011, Linköping, Sweden*, pp. 2985–2992, May 2011, doi: 10.3384/ecp110572985.

[4] "Losses produced by soiling in the incoming radiation to photovoltaic modules - Zorrilla□Casanova - 2013 - Progress in Photovoltaics: Research and Applications - Wiley Online Library." https://onlinelibrary.wiley.com/doi/10.1002/pip.1258 (accessed Feb. 16, 2020).

[5] R. Hammond, D. Srinivasan, A. Harris, K. Whitfield, and J. Wohlgemuth, "Effects of soiling on PV module and radiometer performance," in *Conference Record of the Twenty Sixth IEEE Photovoltaic Specialists Conference - 1997*, Sep. 1997, pp. 1121–1124, doi: 10.1109/PVSC.1997.654285.

[6] L. Micheli and M. Muller, "An investigation of the key parameters for predicting PV soiling losses," *Progress in Photovoltaics: Research and Applications*, vol. 25, no. 4, pp. 291–307, Apr. 2017, doi: 10.1002/pip.2860.

[7] K. K. Ilse, B. W. Figgis, V. Naumann, C. Hagendorf, and J. Bagdahn, "Fundamentals of soiling processes on photovoltaic modules," *Renewable and Sustainable Energy Reviews*, vol. 98, pp. 239–254, Dec. 2018, doi: 10.1016/j.rser.2018.09.015.

[8] K. Sun, L. Lu, Y. Jiang, Y. Wang, K. Zhou, and Z. He, "Integrated effects of PM2.5 deposition, module surface conditions and nanocoatings on solar PV surface glass transmittance," *Renewable and Sustainable Energy Reviews*, vol. 82, pp. 4107–4120, Feb. 2018, doi: 10.1016/j.rser.2017.10.062.

[9] M. Mani and R. Pillai, "Impact of dust on solar photovoltaic (PV) performance: Research status, challenges and recommendations," *Renewable and Sustainable Energy Reviews*, vol. 14, no. 9, pp. 3124–3131, Dec. 2010, doi: 10.1016/j.rser.2010.07.065.

[10] M. S. El-Shobokshy and F. M. Hussein, "Effect of dust with different physical properties on the performance of photovoltaic cells," *Solar Energy*, vol. 51, no. 6, pp. 505–511, Dec. 1993, doi: 10.1016/0038-092X(93)90135-B.

[11] B. Figgis, A. Ennaoui, S. Ahzi, and Y. Rémond, "Review of PV soiling particle mechanics in desert environments," *Renewable and Sustainable Energy Reviews*, vol. 76, pp. 872–881, Sep. 2017, doi: 10.1016/j.rser.2017.03.100.

[12] A. Tsuda, F. S. Henry, and J. P. Butler, "Particle transport and deposition: basic physics of particle kinetics," *Compr Physiol*, vol. 3, no. 4, pp. 1437–1471, Oct. 2013, doi: 10.1002/cphy.c100085.

[13] "Optical and physical properties, time-period, and severity of dust activities as a function of source for the main dust sources of the Middle East - ScienceDirect." https://www.sciencedirect.com/science/article/pii/S136468261830525X (accessed Oct. 10, 2019).

[14] Y. Iwasaka *et al.*, "Pool of Dust Particles over the Asian Continent: Balloon-borne Optical Particle Counter and Ground-based Lidar Measurements at Dunhuang, China," *Environ Monit Assess*, vol. 92, no. 1–3, pp. 5–24, Mar. 2004, doi: 10.1023/B:EMAS.0000014505.43198.48.

[15] "Dust□induced shading on photovoltaic modules - Qasem - 2014 - Progress in Photovoltaics: Research and Applications - Wiley Online Library." https://onlinelibrary.wiley.com/doi/10.1002/pip.2230 (accessed Feb. 16, 2020).

[16] C.-S. Jiang, H. R. Moutinho, B. To, C. Xiao, L. J. Simpson, and M. M. Al-Jassim, "Long-lasting strong electrostatic attraction and adhesion forces of dust particles on photovoltaic modules," *Solar Energy Materials and Solar Cells*, vol. 204, p. 110206, Jan. 2020, doi: 10.1016/j.solmat.2019.110206.

[17] H. R. Moutinho *et al.*, "Adhesion mechanisms on solar glass: Effects of relative humidity, surface roughness, and particle shape and size," *Solar Energy Materials and Solar Cells*, vol. 172, pp. 145–153, Dec. 2017, doi: 10.1016/j.solmat.2017.07.026.

[18] P. Ferrada *et al.*, "Physicochemical characterization of soiling from photovoltaic facilities in arid locations in the Atacama Desert," *Solar Energy*, vol. 187, pp. 47–56, Jul. 2019, doi: 10.1016/j.solener.2019.05.034.

[19] J. J. John, S. Warade, G. Tamizhmani, and A. Kottantharayil, "Study of Soiling Loss on Photovoltaic Modules With Artificially Deposited Dust of Different Gravimetric Densities and Compositions Collected From Different Locations in India," *IEEE Journal of Photovoltaics*, vol. 6, no. 1, pp. 236–243, Jan. 2016, doi: 10.1109/JPHOTOV.2015.2495208.

[20] M. A. Muñoz-García, G. P. Moreda, M. P. Raga-Arroyo, and O. Marín-González, "Water harvesting for young trees using Peltier modules powered by photovoltaic solar energy," *Computers and Electronics in Agriculture*, vol. 93, pp. 60–67, Apr. 2013, doi: 10.1016/j.compag.2013.01.014.

[21] W. Javed, B. Guo, and B. Figgis, "Modeling of photovoltaic soiling loss asa function of environmental variables," *Solar Energy*, vol. 157, pp. 397–407, Nov. 2017, doi: 10.1016/j.solener.2017.08.046.

[22] A. Sayyah, M. N. Horenstein, and M. K. Mazumder, "Energy yield loss caused by dust deposition on photovoltaic panels," *Solar Energy*, vol. 107, pp. 576–604, Sep. 2014, doi: 10.1016/j.solener.2014.05.030.

[23] B. Guo, W. Javed, B. W. Figgis, and T. Mirza, "Effect of dust and weather conditions on photovoltaic performance in Doha, Qatar," in *2015 First Workshop on Smart Grid and Renewable Energy (SGRE)*, Mar. 2015, pp. 1–6, doi: 10.1109/SGRE.2015.7208718.

[24] "Predicting photovoltaic soiling losses using environmental parameters: An update - Micheli - 2019 - Progress in Photovoltaics: Research and Applications - Wiley Online Library." https://onlinelibrary.wiley.com/doi/abs/10.1002/pip.3079 (accessed Feb. 16, 2020).

[25] D. Goossens, "Wind tunnel protocol to study the effects of anti-soiling and anti-reflective coatings on deposition, removal, and accumulation of dust on photovoltaic surfaces and consequences for optical transmittance," *Solar Energy*, vol. 163, pp. 131–139, Mar. 2018, doi: 10.1016/j.solener.2018.01.088.

[26] K. Ilse, M. Z. Khan, N. Voicu, V. Naumann, C. Hagendorf, and J. Bagdahn, "Advanced performance testing of anti-soiling coatings – Part I: Sequential laboratory test methodology covering the physics of natural soiling processes," *Solar Energy Materials and Solar Cells*, vol. 202, p. 110048, Nov. 2019, doi: 10.1016/j.solmat.2019.110048.

[27] M. Piliougine *et al.*, "Comparative analysis of energy produced by photovoltaic modules with anti-soiling coated surface in arid climates," *Applied Energy*, vol. 112, pp. 626–634, Dec. 2013, doi: 10.1016/j.apenergy.2013.01.048.

[28] H. S. Rauschenbach, *Solar cell array design handbook: the principles and technology of photovoltaic energy conversion*. New York: Van Nostrand Reinhold Co., 1980.

[29] M. G. Villalva, J. R. Gazoli, and E. R. Filho, "Comprehensive Approach to Modeling and Simulation of Photovoltaic Arrays," *IEEE Transactions on Power Electronics*, vol. 24, no. 5, pp. 1198–1208, May 2009, doi: 10.1109/TPEL.2009.2013862.

[30] W. De Soto, S. A. Klein, and W. A. Beckman, "Improvement and validation of a model for photovoltaic array performance," *Solar Energy*, vol. 80, no. 1, pp. 78–88, Jan. 2006, doi: 10.1016/j.solener.2005.06.010.

[31] D. Sera, R. Teodorescu, and P. Rodríguez, "PV panel model based on datasheet values," *2007 IEEE International Symposium on Industrial Electronics*, 2007, doi: 10.1109/ISIE.2007.4374981.

[32] S. Silvestre, L. Sentis, and L. Castaner, "A fast low-cost solar cell spectral response measurement system with accuracy indicator," *IEEE Transactions on Instrumentation and Measurement*, vol. 48, no. 5, pp. 944–948, Oct. 1999, doi: 10.1109/19.799652.

[33] "Handbook of Photovoltaic Science and Engineering," *Wiley Online Library*. https://onlinelibrary.wiley.com/doi/book/10.1002/9780470974704 (accessed Dec. 02, 2019).

558

Highlights

1 Soiling process can be reproduced inside a chamber for various ambient conditions
2 Dust load is the main parameter but not the only one affecting soiling effects
3 When the dew point is reached, water channels appear reducing the impact of soiling
4 Spectral-response weighed optical transmission is used for photocurrent prediction
5 Big differences between solar cell and air temperatures decreases soiling

Declaration of interests

☒ The authors declare that they have no known competing financial interests or personal relationships that could have appeared to influence the work reported in this paper.

☐The authors declare the following financial interests/personal relationships which may be considered as potential competing interests:

Mr. Muñoz-García: Methodology, Formal analysis, Investigation, Writing - Original Draft

Mr. Pilat: Validation, Project administration, Resources, Writing - Review & Editing

Mr. Fouris: Methodology, Investigation,Writing - Review & Editing